Cell. Mol. Life Sci. (2016) 73:445–458
DOI 10.1007/s00018-015-2007-y

Cellular and Molecular Life Sciences

ORIGINAL ARTICLE

Protein O-mannosylation is crucial for human mesenchymal stem cells fate

E. Ragni[1] · M. Lommel[2] · M. Moro[3] · M. Crosti[3] · C. Lavazza[1] · V. Parazzi[1] · S. Saredi[4] · S. Strahl[2] · L. Lazzari[1]

Received: 25 March 2015 / Revised: 27 July 2015 / Accepted: 29 July 2015 / Published online: 6 August 2015

Abstract Human mesenchymal stem cells (MSC) are promising cell types in the field of regenerative medicine. Although many pathways have been dissected in the effort to better understand and characterize MSC potential, the impact of protein N- or O-glycosylation has been neglected. Deficient protein O-mannosylation is a pathomechanism underlying severe congenital muscular dystrophies (CMD) that start to develop at the embryonic developmental stage and progress in the adult, often in tissues where MSC exert their function. Here we show that O-mannosylation genes, many of which are putative or verified glycosyltransferases (GTs), are expressed in a similar pattern in MSC from adipose tissue, bone marrow, and umbilical cord blood and that their expression levels are retained constant during mesengenic differentiation. Inhibition of the first players of the enzymatic cascade, POMT1/2, resulted in complete abolishment of chondrogenesis and alterations of adipogenic and osteogenic potential together with a lethal effect during myogenic induction. Since to date, no therapy for CMD is available, we explored the possibility of using MSC extracellular vesicles (EVs) as molecular source of functional GTs mRNA. All MSC secrete *POMT1* mRNA-containing EVs that are able to efficiently fuse with myoblasts which are among the most affected cells by CMD. Intriguingly, in a *pomt1* patient myoblast line EVs were able to partially revert O-mannosylation deficiency and contribute to a morphology recovery. Altogether, these results emphasize the crucial role of protein O-mannosylation in stem cell fate and properties and open the possibility of using MSC vesicles as a novel therapeutic approach to CMD.

Keywords Mesenchymal stem cells · O-Mannosylation · Congenital muscular dystrophy · Differentiation · Extracellular vesicles · *POMT1*

✉ L. Lazzari
lorenza.lazzari@policlinico.mi.it

[1] Cell Factory, Unit of Cell Therapy and Cryobiology, Fondazione IRCCS Ca' Granda Ospedale Maggiore Policlinico, Milan, Italy

[2] Centre for Organismal Studies, Cell Chemistry and Center for Molecular Biology, University of Heidelberg, 69120 Heidelberg, Germany

[3] Istituto Nazionale Genetica Molecolare "Romeo ed Enrica Invernizzi" (INGM), Milan, Italy

[4] Division of Neuromuscular Diseases and Neuroimmunology, Fondazione IRCCS Istituto Neurologico C. Besta, Milan, Italy

Introduction

Human mesenchymal stem cells (MSC) are multipotent progenitor cells responsible for the origin of a variety of tissues in vivo (e.g., paraxial mesoderm: bone, cartilage and striated muscles; lateral plate mesoderm: fat and smooth muscles) and with the potential to differentiate into adipocytes, osteocytes, chondrocytes, tenocytes, and myoblasts in vitro [1, 2]. MSC can be easily isolated from many tissues including adipose tissue [3], bone marrow [4], skeletal muscle [5], deciduous dental pulp [6], synovium [7], Wharton's jelly [8], umbilical cord [9] and umbilical cord blood [10]. In the last years, many reports on both experimental animal models and human clinical trials have shown that MSC may improve tissue repair by secreting different factors (cytokines, proteins, mRNA), either soluble or embedded in extracellular vesicles (EVs), able to regulate a broad range of biological activities including angiogenesis, wound repair, immunity, and defense, as well

as neural activities [11, 12]. In particular, EVs were recently demonstrated to be promising medicinal cargos for different pathologies by their ability to transfer therapeutic RNAs, proteins, or drugs [13].

In the frame of MSC characterization to predict and improve their clinical potential, many pathways defining their identity (differentiation, self-renewal, and immunity) have been dissected with the identification of the structural or enzymatic players. Nevertheless, the impact of protein glycosylation, the most abundant post-translational modification [14], has been neglected. *N*-linked and *O*-linked glycans represent the two major types of glycosylation and are both involved in the maintenance of protein conformation and activity, in protein protection from proteolytic degradation, and in protein intracellular trafficking and secretion [15]. In this view, the role of MSC glycosylation features gets crucial to deeper understand stem cell functionality and fate. Accordingly, a recent report on the major *N*-glycans modulation upon MSC adipogenic differentiation reaffirmed the essential role of protein associated carbohydrate moieties [16].

Among other glycosylation pathways potentially regulating MSC features, O-mannosylation is of particular relevance. Its absence or reduction is a pathomechanism underlying severe congenital muscular dystrophies (CMD) associated with neuronal migration abnormalities, such as Fukuyama CMD, muscle–eye–brain disease, and Walker–Warburg syndrome (WWS) [17]. In humans, O-mannosylation is initiated in the endoplasmic reticulum (ER) by an enzyme complex composed of the protein O-mannosyltransferases POMT1 and POMT2 [18], that recently was demonstrated to be negatively regulated by the 4-diphosphocytidyl-2C-methyl-derythritol synthase ISPD [19]. The *O*-linked mannose residue is then progressed by two alternative protein *O*-linked mannose *N*-acetylglucosaminyltransferases, the ER-resident POMGNT2 (beta 1,4-), or the Golgi POMGNT1 (beta 1,2-), with further processing of these two structures carried out by several enzymes, many of which are verified or putative glycosyltransferases (GTs) [20]. The lack of the branch initiated by POMGNT2 was verified to be directly associated with loss of matrix binding properties of alpha-dystroglycan, part of the dystrophin glycoprotein complex [21]. Such a reduced alpha-dystroglycan functionality leads to weakened anchorage in muscle (e.g., laminin, agrin, and perlecan) and in brain (e.g., neurexin), eventually resulting in CMD phenotypes [22].

In this work, our efforts have been focused on dissecting the importance of *O*-mannosylated glycans in MSC fate and properties. First, we analyzed the expression pattern of the O-mannosylation cascade initial genes, *ISPD* and *POMT1*/2, together with both several components of the alpha-dystroglycan activating *POMGNT2* branch, *POMGNT2-B3GNT2-POMK-FKTN-FKRP-B4GAT1-LARGE,* and *LARGE2* [23–25], and the first genes of the alternative *POMGNT1* pathway, *POMGNT1-GNTIX* [26, 27]. Then, we studied gene modulation during mesengenic differentiation and the effects of the inhibition of the first steps of the pathway on MSC properties and differentiation potential. Finally, we investigated a possible role for MSC EVs as an innovative therapeutic approach for CMD.

Materials and methods

Cell isolation and growth

MSC from lipoaspirate (ADMSC), bone marrow aspirate (BMMSC), and umbilical cord blood (CBMSC) were obtained from healthy donors after informed consent [3, 10, 28]. MSC were propagated in alpha MEM supplemented with 20 % FBS (Life Technologies, Carlsbad, CA, USA). Stem cell identity of isolated ADMSC, BMMSC, and CBMSC was assessed by immunophenotype profiling that confirmed high expression of typical MSC cell-surface antigens, such as CD90, CD73, CD44, and CD105, and negativity for hemato-endothelial markers such as CD34, CD133, and CD45, following what reported in [28] (data not shown).

Fibroblasts (HSF) were obtained from skin biopsies of healthy donors after informed consent. Briefly, after removal of subcutaneous fat and connective tissue (hypodermis), the epidermis and dermis were minced and incubated with Dispase (Roche Applied Science, Mannheim, Germany) overnight at 4 °C. Then, the dermal part was separated from the epidermis and minced in 1–2 mm diameter pieces that were placed in dishes in alpha MEM plus 10 % FBS. After 14–21 days, fibroblast colonies were detached and re-seeded at 4000 cells/cm^2.

Healthy myoblasts were a kind gift of Stefania Corti (Neuralstemlab, Università degli Studi di Milano). *pomt1* (hetero. C.1611C>G Ser537Arg/c.1770G>C Gln590His) myoblasts (from the biobank "Cells, tissues and DNA from patients with neuromuscular diseases" of the Besta Neurological Institute, Milano, Italy) were obtained from a WWS male patient that died at 2 years old. For mutation screening, primers were designed flanking the intron–exon junctions of each *POMT1* exon and the 3′UTR, based on published sequences (GenBank accession number: NM_007171.2). PCRs were performed with Mega Mix Double (Microzone, Haywards Heath, West Sussex, UK). The products were purified using microCLEAN (Microzone, Haywards Heath, West Sussex, UK) and sequenced directly with the BigDye Terminator v1.1 Cycle Sequencing Kit (Applied Biosystems, CA, USA). Sequences were analyzed on an ABI Prism 3100 Genetic

Analyzer (Applied Biosystems, CA, USA) with Seqscape V2.5 software (Applied Biosystems). All myoblasts, both healthy and *pomt1*, were cultured in DMEM supplemented with 20 % FBS, 1 % penicillin–streptomycin, 2 mM L-glutamine, 10 μg/ml insulin (Sigma–Aldrich, St. Louis, MO, USA), 2.5 ng/ml basic fibroblast growth factor (bFGF; Gibco, Paisley, Scotland), and 10 ng/ml epidermal growth factor (EGF; Gibco).

All subsequent studies on cell growth were carried out in technical duplicate on three independent cell lines for BM- and ADMSC, four cell lines for CBMSC and fibroblasts and two cell lines for control healthy myoblasts. Experiments were performed at passage 5. For POMT1/POMT2 inhibitor studies, culture medium was supplemented with 0.1 % DMSO or R3A-5a (Biotrend GmbH, Cologne, Germany) dissolved in DMSO and changed each 3 days.

Mesengenic differentiation and biochemical quantification

MSC were seeded in duplicate in 6-well plates at a concentration of 2×10^4 cells/cm^2 in 2 mL of media and cultured in control medium (alpha MEM supplemented with 20 % FBS) until 70–80 % confluence when differentiation was performed as previously reported [29]. To promote myogenic induction, the SkGM-2 BulletKit (Lonza GmbH, Cologne, Germany), a commercial basal medium for MSCs which includes pro-myogenic factors that induce myogenic induction, was used. For quantification of differentiation at the end of the process (3 weeks), to detect adipogenesis, cells were fixed in 4 % formaldehyde and stained for 1 h with Oil Red O (Sigma–Aldrich, St. Louis, MO, USA) (0.3 % in 60 % isopropanol). Incorporated Oil Red O was dissolved in isopropanol and detected at 520 nm. For osteogenesis, cultures were fixed in 70 % ethanol and incubated with Alizarin Red solution (2 g/100 mL in distilled water, Sigma–Aldrich) for 15 min. Alizarin Red was recovered with 10 % acetic acid, the solution neutralized with 10 N NaOH and extracted Alizarin Red measured at 405 nm. For chondrogenesis, chondrogenic cultures were fixed in 4 % formaldehyde, and then stained with Alcian Blue (1 g/L in 0.1 M HCl, Sigma–Aldrich) for 6 h. To recover Alcian Blue, dry wells were covered with 6 N Guanidine HCl (Sigma–Aldrich) and the amount of extracted dye measured at 650 nm.

For RNA extraction, cells were collected at day 0, as pre-induction condition, and at day 7, to harvest MSC actively differentiating. For inhibitor studies, culture medium was supplemented with 0.1 % DMSO or R3A-5a in DMSO.

RNA isolation and cDNA synthesis and quantitative RT-PCR assays

RNA was isolated using the RNeasy Mini kit (Qiagen, Hilden, Germany) following manufacturer's instructions. RNA purity was determined by measuring the absorbance A260/A280 in a Nanodrop spectrophotometer. RNA integrity was assessed using electrophoretic techniques.

Quantitative PCR was carried out using "SsoFast EvaGreen Supermix" (Bio-Rad Laboratories, Hercules, CA, USA). cDNA derived from 800 ng RNA and gene specific primers (*ISPD*, *POMT1*, *POMT2*, *POMGNT1*, *POMGNT2*, *B3GNT2*, *POMK*, *GNTIX*, *FUKUTIN*, *B4GAT1*, *LARGE*, *FKRP*, *LARGE2*, *DAG1*, *PPARG*, *OPN*, *SOX5,* and *DMD*) were used. Triplicates of all reactions were analyzed and within each triplicate values exceeding standard deviation >10 % were discarded. Each assay also included a blank. To confirm product specificity, a melting curve analysis was performed after each amplification. Relative gene expression was normalized to *TBP* or *RPLP0* [29] expression using the $\Delta\Delta C_t$ method. For statistical analysis and expression data generation, the Bio-Rad CFX Manager software was used. Primer sequences will be provided upon request.

EVs preparation

MSC were grown to 80 % confluence, and then fresh medium without FBS was added. After 24 h, conditioned culture medium was collected and serially centrifuged to remove floating cells and cellular debris ($400\times g$ for 10 min, $600\times g$ for 10 min and $5000\times g$ for 15 min for 3 times) before being ultracentrifuged at $100{,}000\times g$ for 1 h at 4 °C. The pellet was suspended in PBS or dissolved in lysis buffer for RNA extraction.

Measurement of particle number and size distribution by nanoparticle tracking analysis (NTA)

NTA was carried out using the Nanosight system (NanoSight, Wiltshire, UK) on EVs suspended in PBS that were further diluted 50-fold for analysis. NTA related the rate of Brownian motion to particle size. Vesicles were visualized by light scattering using a conventional optical microscope aligned perpendicularly to the beam axis. After a video was taken, the NTA software tracked between frames the Brownian motion of individual vesicles and calculated total concentration and their size through application of the Stokes–Einstein equation.

EVs transfer and glycosylation restoration assessment

250×10^9 EVs isolated from the serum-free supernatant of 100×10^6 BMMSC were supplemented to the growth medium of approximately 25,000 *pomt1* myoblasts with or without *POMT1* siRNA pre-loading through 5 daily administrations. PBS was used as negative control in a parallel cell culture. Two independent BMMSC lines were used. At the end of the 5th day, a previously published flow cytometry protocol was followed to detect the amount of glycosylated α-DG [30]. Briefly, cells were incubated with mAb IIH6 (1:100; Merck Millipore, Darmstadt, Germany). Incubation was for 2 h on ice. Cells were then washed twice and labeled with FITC-conjugated goat secondary antibodies (1:200; Abcam, Cambridge, UK) for 1 h on ice in the dark. After two wash-steps, cells were analyzed with a FACSCanto instrument (Becton–Dickinson). At least 15,000 events were acquired. Image analysis was done using FloJo software (Tree Star, Ashland, OR). ΔMFI values were calculated as MFI of stained cells subtracted of MFI of unstained cells. MFI of control cells was set around 10^2.

siRNA transfection

In a 24 well tissue culture plate, 2.5×10^4 myoblasts (healthy or *pomt1*) were incubated per 24 h and then transfected with *POMT1* or scramble-FITC siRNA (both from Santa Cruz Biotechnology, CA, USA) following manufacturer's protocol. Briefly, 24 pmol siRNA were suspended in 0.320 mL siRNA Transfection Medium (60 nM final) and cells incubated for 24 h. After 24 h, siRNA was removed and cells were washed and incubated with muscle cell medium (Lonza) for 5 days and analyzed by qRT-PCR (5 days) or FACS (24 h). For EVs treatment, after removal of transfection medium, EVs were supplemented each 24 h as previously mentioned. *POMT1* mRNA reduction was assessed by qRT-PCR as previously described. Scramble-FITC transfection efficiency was measured via FACS on a FACSCanto flow cytometer (at least 30,000 events were acquired).

PKH26-labeled EVs transfer

EVs were labeled with PKH26 (Sigma–Aldrich), according to the manufacturer's protocol, with some modifications. Briefly, EVs were suspended in 0.3 mL Diluent C. Separately, 0.3 mL Diluent C was mixed with 1.5 μL PKH26. The EVs suspension was mixed with the stain solution and incubated for 20 min at room temperature in the dark. The labeling reaction was stopped by adding an equal volume of 1 % BSA in PBS and a solution containing 0.5 mg/mL DAPI (Sigma–Aldrich) was added to label nuclear DNA. Labeled EVs were ultracentrifuged at $100{,}000 \times g$ for 1 h at 4 °C, washed with PBS-1 % BSA, ultracentrifuged again and finally suspended in PBS. Labeled vesicles were incubated with *pomt1* myoblasts in a 10,000: 1 ratio. PBS that received the same treatment as above was used as a control. The cells were analyzed by flow cytometer with a FACSCanto instrument. Image analysis was done using FloJo software.

Western blot analysis

For glyco alpha-dystroglycan analysis, a protocol previously published in [19] was followed. Briefly, from cell extracts of $1.5–2 \times 10^6$ cells, alpha-dystroglycan-complex was enriched by WGA-lectin precipitation and proteins were separated on SDS-PA gel. The immunoblot was decorated with IIH6 mouse monoclonal antibodies.

Cell viability assessment

To detect viable cells after inhibitor treatment, MSC were detached with Tryple enzyme (Life Technologies) and washed with PBS. To collect any possible detached cell in the culture supernatant, conditioned medium was centrifuged at high speed (5000 rpm) and pellet, although never visible, suspended, and added to enzyme detached cells. After a further centrifugation step, total cells were suspended in binding buffer and 1/20 volume propidium iodide (20 μg/mL; Bender MedSystems GmbH, Vienna, Austria) was added. All solutions were filtered three times with 0.1 μm filters to reduce debris contamination. Labeled cells were immediately analyzed on a FACSCanto flow cytometer that was previously set in the physical parameters to exclude debris still present in the filtered suspension solution. At least 30,000 events were acquired with no further gates. Image analysis was done using FloJo software. Cell viability was also confirmed via Trypan Blue staining by preparing a 1:1 dilution of the cell suspension using a 0.4 % Trypan Blue (Lonza) solution. Viable cells were counted under a microscope and cell viability was expressed as the viable cell numbers/total cell numbers multiplied by 100.

Results

O-mannosylation related genes modulation in MSC

To explore the role of the pathways leading to protein O-mannosylation in mesenchymal stem cells, the expression levels of *ISPD*, *POMT1*, *POMT2*, *POMGNT1*, *POMGNT2*, *GNTIX*, *B3GNT2*, *POMK*, *FUKUTIN*, *FKRP*,

B4GAT1, *LARGE*, and *LARGE2* (Fig. 1) have been assayed in MSC from two adult sources, BMMSC and ADMSC, and one fetal source, CBMSC, via qRT-PCR (Fig. 2a–c). An absolute C_t value of 35 was set as the maximum threshold for reliable quantification and, based on previous experience in our laboratory, a C_t lower than 20 assumed for highly expressed genes (e.g., Actin beta), between 20 and 30 for medium abundant transcripts (e.g., Glucuronidase beta), and higher than 30 for low expressed ones. Based on these criteria, for all cell types under study all genes laid in the medium expressed range with only *GNTIX* always showing a C_t value closer to 35 and *LARGE2* higher than the threshold. Setting as 1 the normalized amount of *POMT1*, for all MSC a similar pattern of expression was verified with *POMT2* always being expressed at 50 % levels of its enzymatic complex partner counterpart. Analyzing the ratio of the alternative *POMGNT1* and *POMGNT2* genes, *POMGNT1* resulted to be 3.5–4 times more expressed. Taken together, these data show a very similar behavior for MSC of different origins with a preferentiality for POMGNT1 branch.

Then, to verify if this transcription profile is maintained also in somatic cells directly deriving from MSC, mRNA levels were measured in skin fibroblasts (HSF) and myoblasts (Fig. 2d–e). A global pattern of expression similar to those obtained in MSC was observed. The major differences were a 4- to 10-fold (depending on the MSC type) higher expression for *GNTIX* in HSF and a 5- to 12-fold higher presence of *LARGE2* mRNA in HSF and myoblasts, although in both cells *LARGE2* C_t values remained higher than 35. Notably, comparing *POMGNT1* and *POMGNT2* mRNA, in myoblasts a ratio close to 1 was observed (Fig. 2f) due to a nearly 5 times higher *POMGNT2* transcript amount. This increase, despite the absence of significant modulation in alpha-dystroglycan coding gene *DAG1* mRNA, is thus a specific myoblast trait to promote alpha-dystroglycan activity, which is crucial for muscle functionality. Consistently, *POMGNT1*/*POMGNT2* ratio further decreased to 0.5 in myotubes (Fig. 2f), a terminal differentiation of myoblasts, due to a 15–20 times higher *POMGNT2* mRNA amount. Further, to explore the effects of *POMGNT2* modulation on alpha-dystroglycan, we performed a Western Blot using an antibody (IIH6, see "Materials and methods") specific for an uncharacterized O-mannosidically linked carbohydrate epitope. Notably (Fig. 2g), with respect to BMMSC, glycosylated alpha-dystroglycan molecular weight increased in both myoblasts and myotubes, confirming that *POMGNT2* branch modulation leads to the appearance, or most probably the increase, of highly glycosylated forms that are almost undetectable in MSC.

Gene modulation was further monitored during adipogenic, osteogenic, chondrogenic (AOC), and myogenic induction (Fig. 3a–d) in two independent MSC lines. One week after induction and therefore in a condition of actively differentiating MSC, no major differences (>2-fold modulation Induced/CTRL, p value < 0.05 in both tested cell lines) were detected in AOC processes, whereas during myogenesis a significant (4 times, p value < 0.05 in both independent cell lines) increase in *POMGNT2* mRNA

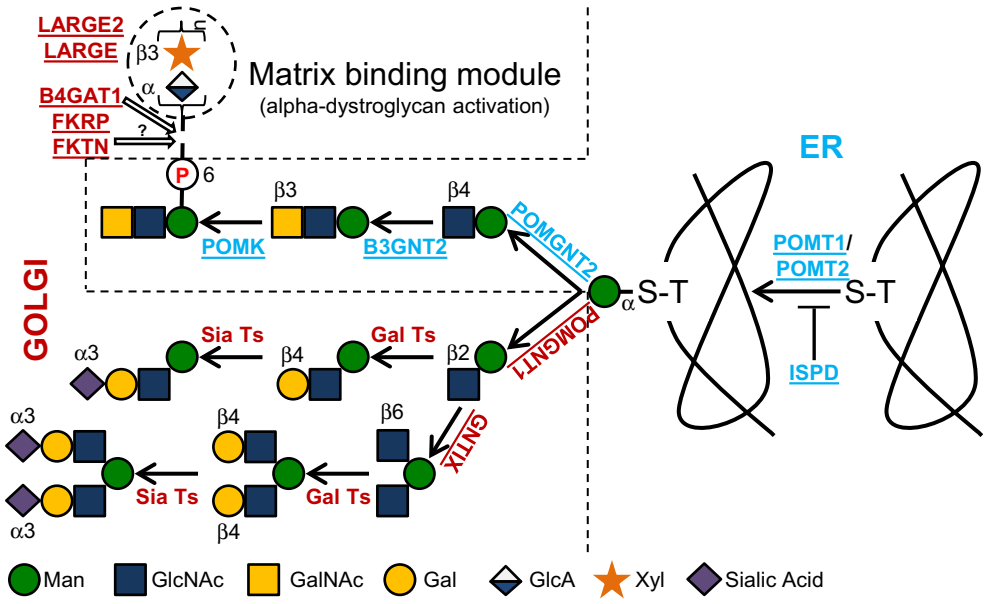

Fig. 1 Simplified cascade of the enzymes/proteins involved in the O-mannosylation pathway showing the alternative *POMGNT1* and *POMGNT2* (alpha-dystroglycan activating) branches. Assayed genes are underlined. *S/T* serine and threonine. For a more complete picture, please refer to Endo (2015)

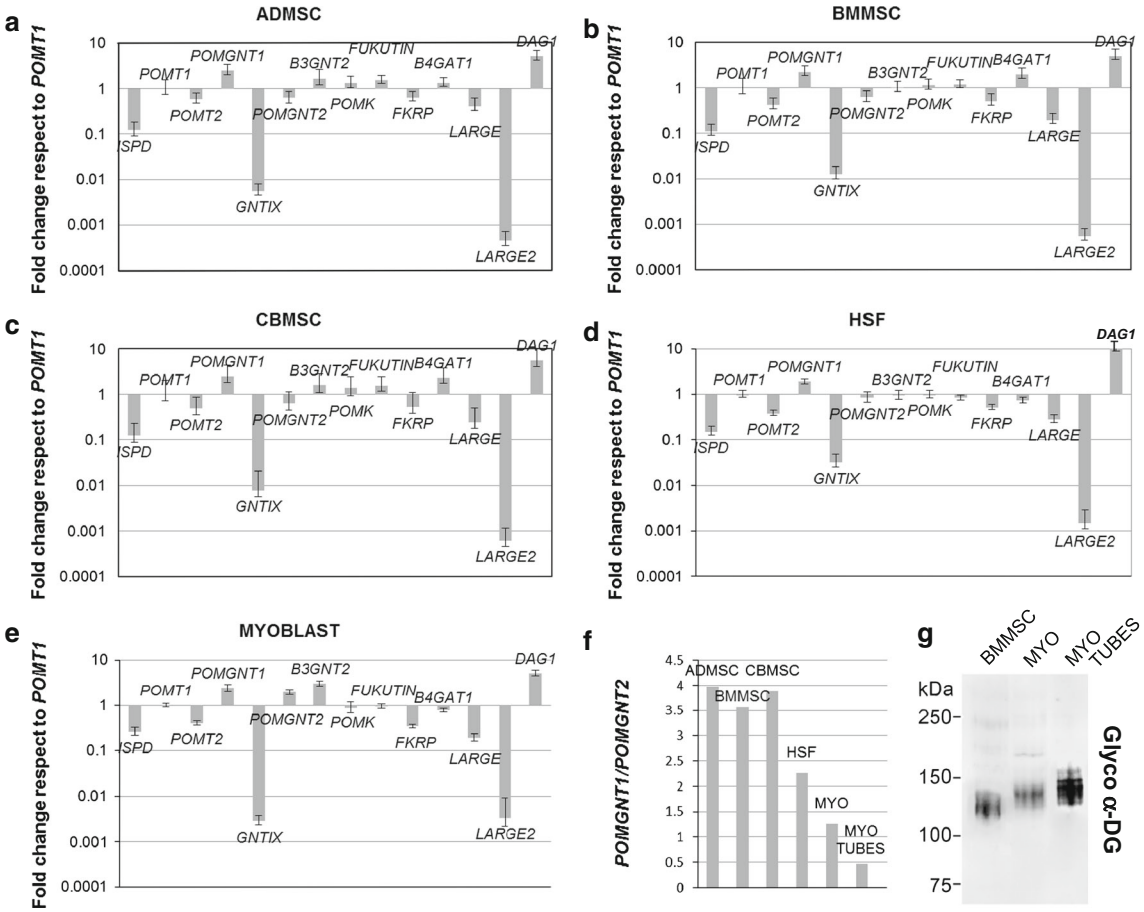

Fig. 2 Ratio of expression of O-mannosylation-associated genes with respect to *POMT1* set as 1. Expression in **a** MSC from adipose tissue, **b** MSC from bone marrow, **c** MSC from umbilical cord blood, **d** fibroblasts, and **e** healthy myoblasts. In **f**, *POMGNT1*/*POMGNT2* expression ratio is shown. *Error bars* represent SD ($N > 3$). **g** Analysis of alpha-dystroglycan glycosylation using an antibody (IIH6) specific for an uncharacterized O-mannosidically linked carbohydrate in bone marrow MSC (BMMSC), myoblasts (MYO), and myotubes (MYOTUBES)

was detected. Such results are in agreement with the *POMGNT2* increase observed in myoblasts, thus reinforcing the notion of a differential alpha-dystroglycan activation needed not only for muscle function but also for muscle development that, when missing, is a major causal agent of CMD.

O-mannosylation is crucial for MSC fate and mesengenic potential

To explore the role of O-mannosylation on MSC fate, we inhibited POMT enzymatic activity using a Rhodanine-3-acetic acid derivative, such as compound 5a (R3A-5a), which was demonstrated to be an in vitro and in vivo highly specific inhibitor of both fungal and mammalian protein O-mannosyltransferases [31–33]. R3A-5a treated MSC exhibited a proliferation reduction with cell number around 30–40 % of the control condition at 6 days, without signs of cell detachment (Fig. 4a). No cytotoxic effects at 6 days were observed by PI staining (Fig. 4b) and similar results were obtained by Trypan Blue staining (data not shown). Still, cells became disorganized, rounder, and enlarged losing the fibroblast-like shape typical of MSC (Fig. 4c–h). Effective block of O-mannosylation was then confirmed by Western Blot using the IIH6 antibody (Fig. 4i). Notably, qRT-PCR analysis of GTs did not show any R3A-5a effect on the transcript levels (data not shown).

We further investigated the effect of O-mannosylation inhibition during AOC and myogenic induction in vitro. At the end of the adipogenic process, R3A-5a treatment reduced both the number and the size of newly generated lipid droplets, stained with Oil Red O dye (Fig. 5a), that are indicators of positive differentiation into adipocytes. Biochemical quantification of the incorporated dye showed a reduction higher than 50 % (Fig. 5b). Efficiency of the osteogenic conversion was monitored analyzing the deposition of calcium-phosphate, an indicator of MSC differentiation into osteocytes, with the specific dye

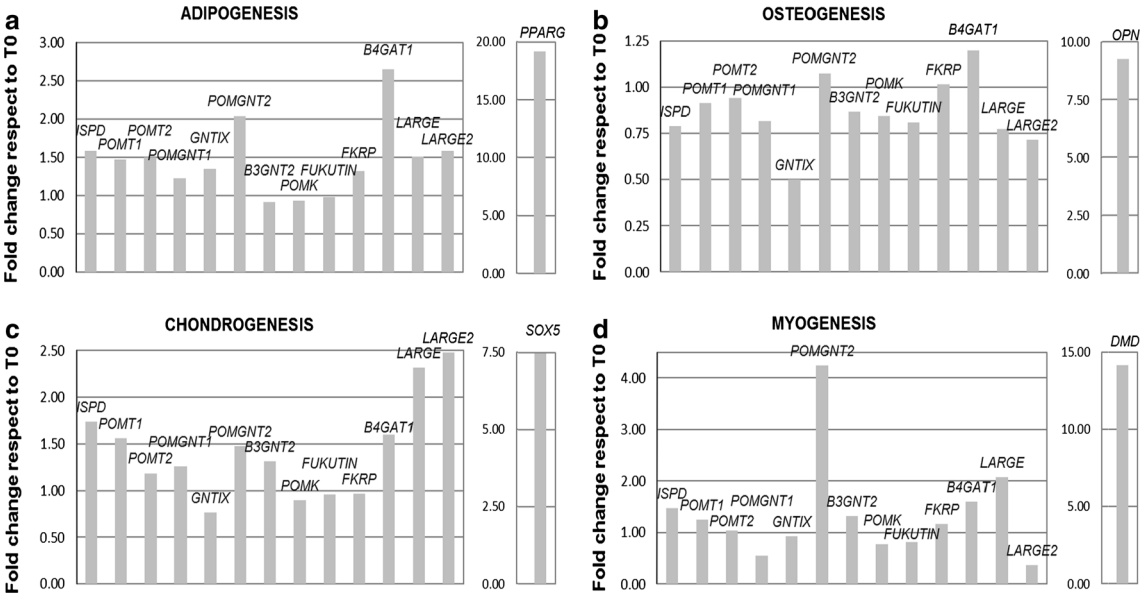

Fig. 3 Expression ratio of O-mannosylation associated genes under mesengenic commitment with respect to undifferentiated cells. Expression during **a** adipogenesis, **b** osteogenesis, **c** chondrogenesis, and **d** myogenesis. For each process, the increase of a specific marker (*PPARG*, *OPN*, *SOX5* and *DMD*) to confirm active differentiation induction is shown. Mean of the values obtained in two independent cell lines tested, three times each, after verification that the modulation values of each gene after induction were not statistically different between the two cell lines (Student's *t* test *p* value > 0.05)

Alizarin Red (Fig. 5c). Block of O-mannosylation led to a 60 % increase of dye incorporation (Fig. 5d) indicating an enhanced osteogenic potential. Further, the chondrogenic differentiated state of MSC was followed with Alcian Blue, a dye-staining acid mucosubstances (sulfated and carboxylated mucopolysaccharides) present in cartilage tissues (Fig. 5e). Quantification of incorporated dye showed complete absence of differentiation in presence of the inhibitor with symptoms of cell suffering such as granulation of the cytoplasm and eventually detachment (Fig. 5f). Finally, inhibitor supplementation during myogenic induction led to a sudden (24 h) cell death (Fig. 5g). To confirm the crucial interplay between O-mannosylation and myogenic phenotype, human healthy myoblasts were treated with R3A-5a and also in this case cell death was observed at 24 h (Fig. 5h). Altogether, these data suggest that impaired O-mannosylation affects MSC differentiation potential with particular relevance on the myogenic commitment where properly activated O-mannosylated players are crucial for muscle cell function.

MSC-EVs as shuttle for therapeutic mRNA

Recently, EVs were demonstrated to be promising cargos for the delivery of drugs, proteins and RNAs [13]. In this perspective, we decided to characterize MSC EVs in order to verify their feasibility as vehicle of wild-type GTs mRNA to CMD cells.

First, EVs were isolated by ultracentrifugation at 100,000×*g* from the culture medium after 24 h FBS starvation to abolish serum-EVs contamination (see "Materials and methods"). Of note, starvation did not increase the amount of apoptotic or dead cells (for BMMSC, 1.6 % ± 0.6 PI positive cells after starvation vs 1.1 % ± 0.8 with FBS). EVs physical properties were analyzed by Nanoparticle Tracking Analysis (NTA) (Fig. 6a), able to characterize in number and dimension lipid nanoparticles ranging from 10 to 2000 nm. For all three MSC, the EVs size distribution was similar, ranging from 50 to 350 nm with a peak at 130–150 nm and a mean size around 200 nm (Fig. 6b). The EVs yield per 10^6 MSC was similar and around 1–3 × 10^9 particles per day. A similar number was also observed when platelet lysate (PL), a powerful inducer of MSC proliferation, was used in place of FBS (EVs/cell ratio for PL vs FBS = 0.9 ± 0.2). Thus, all MSC-EVs are similar in both number and physical features.

Second, being *POMT1* associated with the most severe CMD forms and thus an optimal candidate for future therapeutic approaches, the presence of its transcript was confirmed in isolated EVs by RT-PCR (Fig. 6c). To corroborate the notion of mRNA presence inside the vesicles and not just membrane-bound on the external surface, isolated EVs were further RNAse A treated. No decrease in the amount of the transcripts was noticed confirming that isolated EVs are both intact and that *POMT1* transcripts are engulfed in EVs lumen.

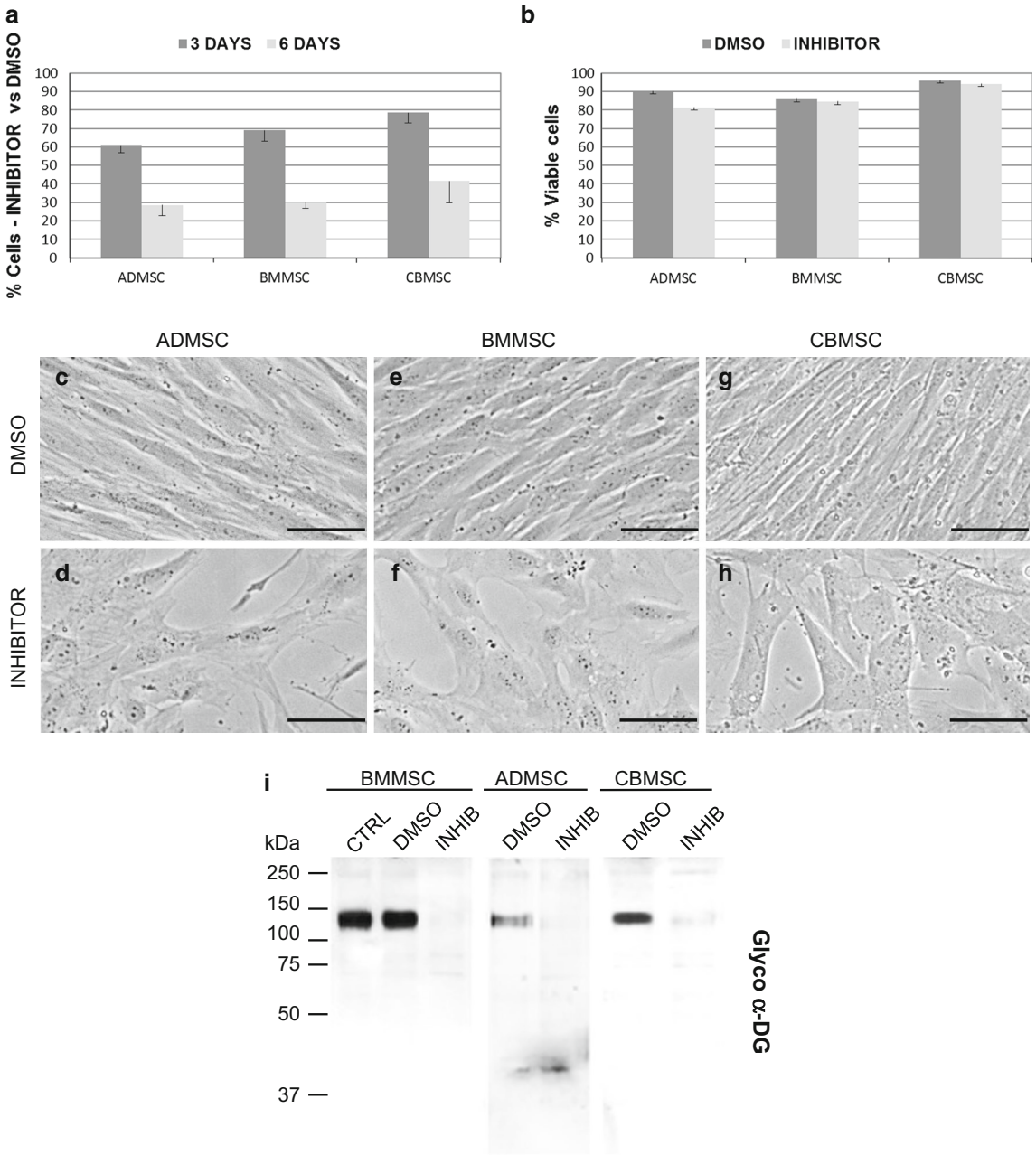

Fig. 4 POMTs inhibitor effect on MSC. **a** Reduction in cell proliferation and number after 3- and 6-days 50 μM incubation with respect to 0.1 % DMSO mock-treated MSC, and **b** percentage of viable cells after 6-days inhibitor treatment measured as propidium iodide negative cells. *Error bars* represent SD ($N = 3$). **c**–**h** Effects of R3A-5a on MSC morphology. *Scale bars* 20 μM. **i** alpha-Dystroglycan glycosylation abolishment after 3-days 50 μM inhibitor incubation in MSC using an IIH6 antibody

Third, to choose the best MSC type as source of therapeutic EVs, we compared the amount of *POMT1* mRNA in the three MSC vesicles, using the number of EVs processed for RNA extraction to normalize qRT-PCR data due to the lack of reliable EVs mRNA housekeepers (Fig. 6d). No significant (p value > 0.05) differences were detected. A rough estimation indicated that for all sources *POMT1* mRNA included in 100×10^9 EVs is equivalent to mRNA that can be extracted from 500 to 1000 cells. Similar *POMT1* mRNA amount was recovered in EVs originated from MSC pre-grown in platelet lysate (*POMT1* mRNA/EVs ratio for PL vs FBS $= 1.2 \pm 0.1$). Finally, we directly stained the vesicles with membrane label PKH26 and examined whether they were able to be incorporated by myoblasts, among the most affected cell types in CMD. After 24 h of incubation, vesicles were detected in the cytoplasm in a punctuate pattern (Fig. 7a), with FACS analysis showing no major incorporation differences

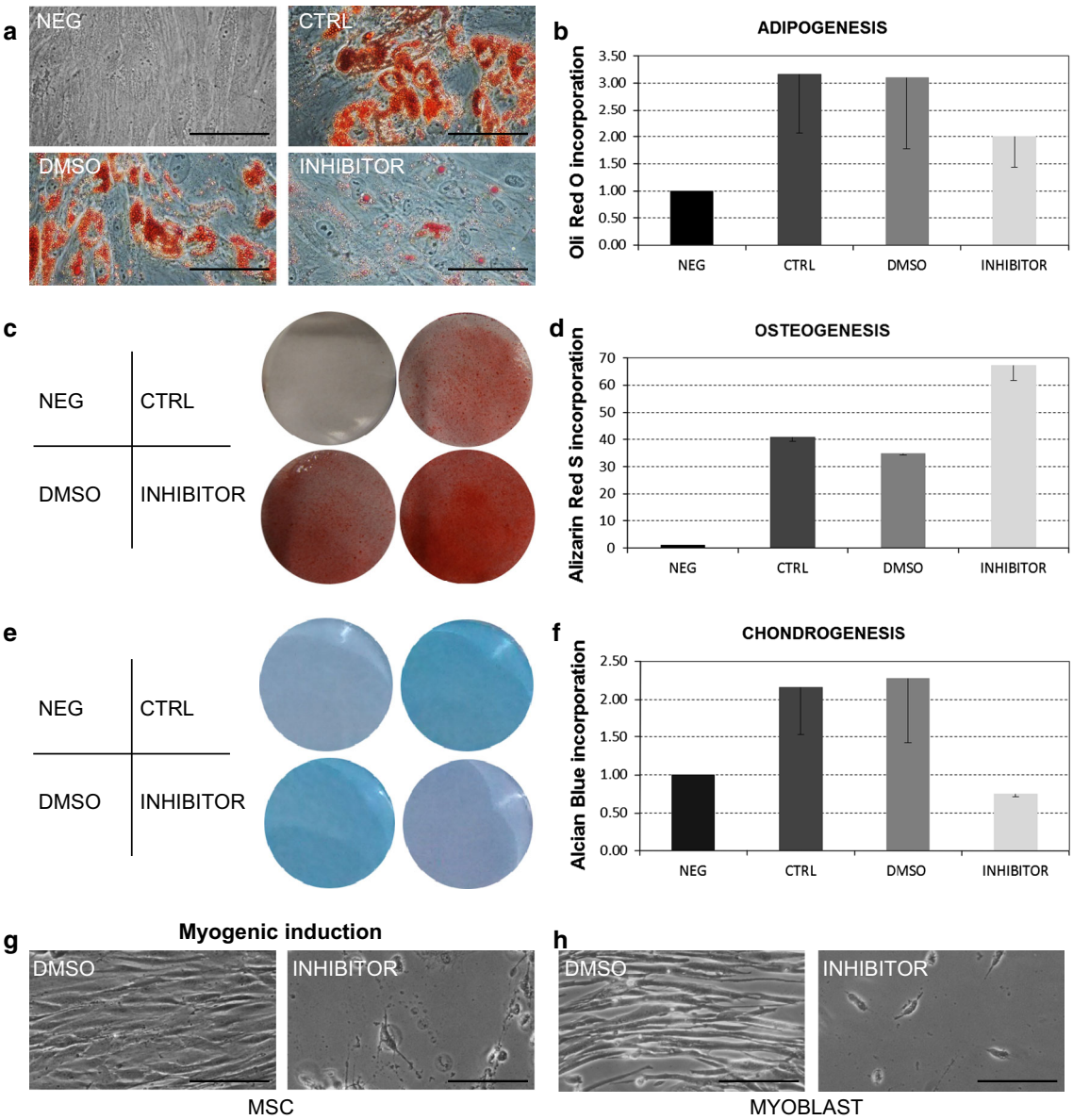

Fig. 5 Inhibitor effect on MSC differentiation potential. **a** R3A-5a inhibition of adipogenesis. *Oil red* O staining of lipid droplets in non-induced ADMSC (NEG), induced (CTRL), induced + DMSO (DMSO) and induced + R3A-5a (INHIBITOR). *Scale bars* 20 μM. **b** Relative ratios of *Oil Red* O levels to levels in non-induced MSC (mean of two independent cell lines; *bars*, SD). **c** R3A-5a enhancement of osteogenesis. *Alizarin red* staining of calcium deposits. **d** Relative ratios of *Alizarin red* levels. **e** R3A-5a complete block of chondrogenesis. *Alcian blue* staining of mucopolysaccharides. **f** Relative ratios of *Alcian blue* levels. **g** Inhibitor effect on MSC after 1-day incubation under myogenic-induction conditions and **h** R3A-5a outcome on healthy myoblasts after 1-day treatment. *Scale bars* 20 micron

between EVs from different sources (Fig. 7b). These data confirm similar cargo content, at least for *POMT1* transcript, and fusion properties for all MSC EVs under study.

BMMSC-EVs for CMD myoblasts recovery

Due to similar EVs content and properties, we decided to study the ability of BMMSC-EVs (250 billion, equivalent to the *POMT1* mRNA content of 2500 cells) to donate wild-type *POMT1* mRNA to myoblasts (25,000 cells) obtained from a WWS patient with both *POMT1* alleles mutated (see "Materials and methods"). With respect to control myoblasts from healthy donors, patient cells displayed a rhomboid and disorganized morphology (Fig. 7c). After EVs administration, *pomt1* cells acquired an elongated shape and an organized disposition in fibers-resembling structures similar to those observed in healthy myoblasts (Fig. 7c). To associate these result with a

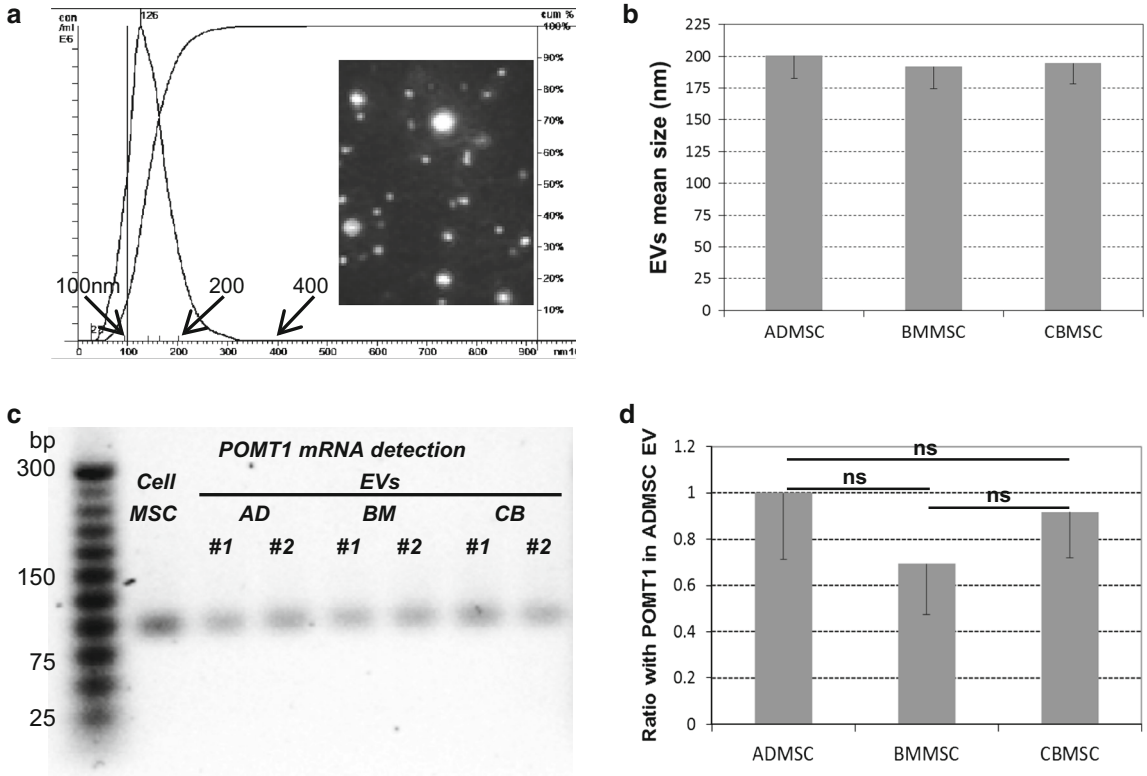

Fig. 6 EVs properties. **a** Representative size distribution of CB-MSC EVs as measured by NTA together with a typical NTA generated image of analyzed vesicles. **b** Mean diameters of EVs produced by MSC, determined by NTA. *Error bars* represent SD ($N > 3$). **c** Confirmation by RT-PCR of *POMT1* mRNA presence in EVs through direct comparison with cell pellet amplification. *Left lane*, DNA Molecular Weight markers with indication of bp length. **d** Relative mRNA levels of *POMT1* in MSC EVs after normalization to *POMT1* mRNA in ADMSC. *Error bars* represent SD ($N = 7$). *ns* not significant

rescued O-mannosylation activity, we analyzed the glycosylation status of alpha-dystroglycan with IIH6 Ab by FACS [30]. In *pomt1* mutant myoblasts, we detected significantly reduced levels of alpha-dystroglycan glycosylation (ΔMFI, calculated as Ab stained MFI—unstained MFI, value of 17 ± 2, that is 6 ± 1 % of control myoblasts having a ΔMFI value of 283 ± 15). This was consistent with the results observed in *pomt1* patient fibroblasts that showed a strong reduction of the glycoepitope [30]. Most importantly, EVs supplementation resulted in a partial recovery of the glycosylated alpha-dystroglycan (ΔMFI value of 42 ± 4, p value with *pomt1* myoblast of 0.02, 2 independent EVs administration, each from two independent BMMSC isolates). Therefore, the amount of activated alpha-dystroglycan, although being still 16 % of control myoblasts, resulted to be 250 % of untreated patient cells.

To unravel whether such low increase in POMT1 activity is the only responsible for the morphology recovery observed in *pomt1* myoblasts, we decided to load patient cells with a *POMT1* siRNA before EVs administration in order to degrade newly EVs-transferred *POMT1* transcript. In this way, all the other EVs-embedded molecules and potentially contributing to the phenotype recovery would be still present. To verify siRNA transfection protocol feasibility, in a pilot experiment we first studied scramble-FITC siRNA transfection efficiency in healthy myoblasts and obtained 80 % positive cells after 24 h. Second, using the specific *POMT1* siRNA, after 5 days a nearly 80 % reduction of *POMT1* mRNA and a 40 % reduction of alpha-dystroglycan glycosylation (ΔMFI value of 180 ± 12) were obtained. Finally, EVs were administrated to pre-loaded *pomt1* cells as previously described. Interestingly, cells showed a disposition in fibers-resembling structures with an elongated shape, although not as narrow as healthy cells (Fig. 7c), indicating a good degree of morphology recovery. FACS analysis showed very low levels of alpha-dystroglycan glycosylation that were not significantly different from untreated *pomt1* cells (ΔMFI value of 24 ± 3, p value with *pomt1* myoblasts of 0.1), meaning that siRNA pre-administration efficiently interfered with newly transferred *POMT1* mRNA stability and translation. Thus, amelioration in patient cells morphology upon EVs treatment is only in part due to POMT1 activity restoration suggesting that other players may be involved.

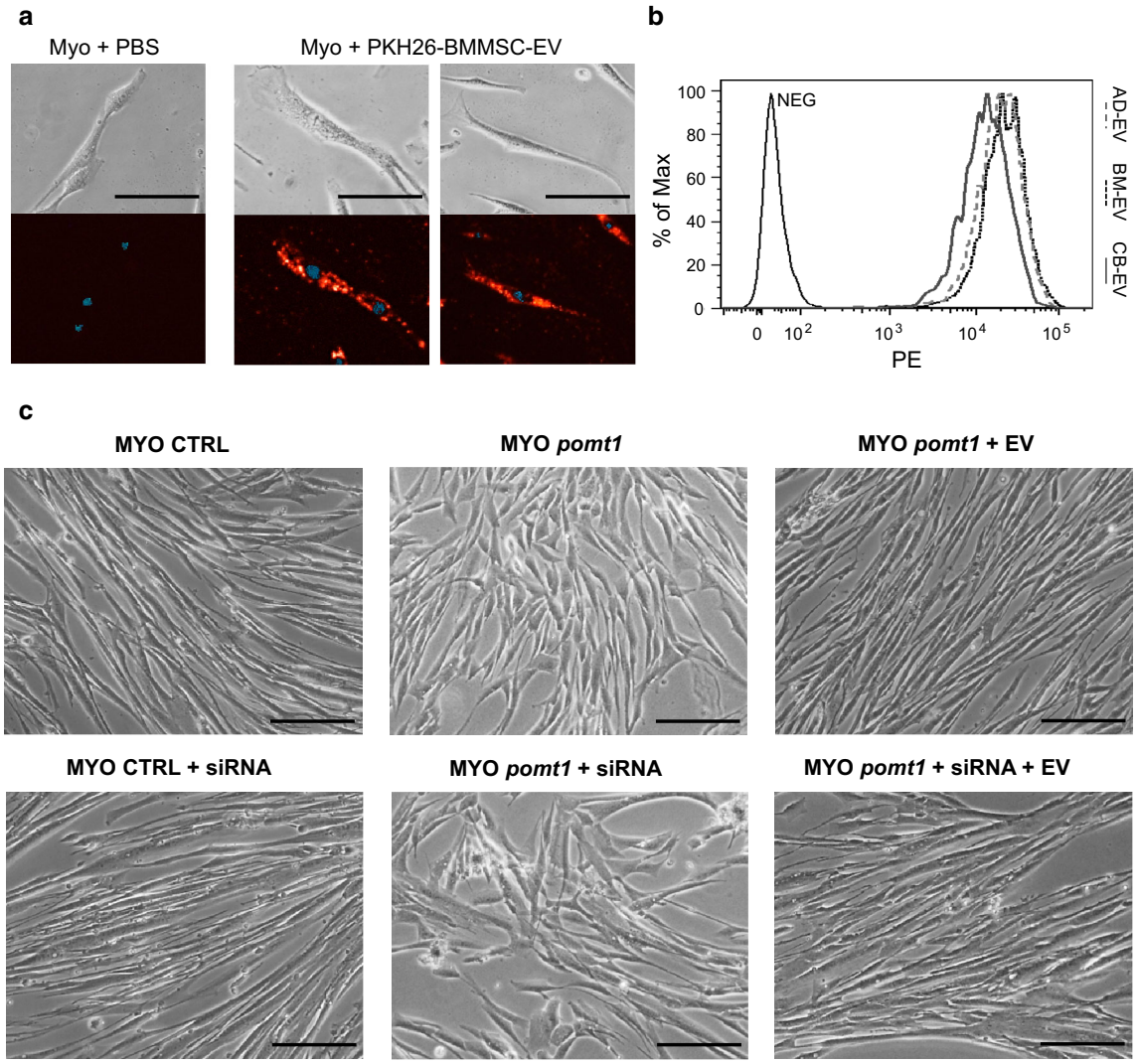

Fig. 7 Effects of EVs-associated *POMT1* mRNA transfer. **a** Representative images of myoblasts cultured with either PBS or PKH26 labeled-EVs from BMMSC showing incorporation in a punctuate fashion after 24 h. *Blue dots*, DAPI nuclear staining. *Scale bars* 40 μM. **b** EVs from different MSC are incorporated in similar amounts in healthy myoblasts after 24 h. **c** BMMSC-EVs supplementation to *pomt1* patient myoblasts is able to revert the unorganized and rhomboidal cell morphology in a healthy myoblast-like ordered disposition of cells together with an increased cell size and elongated morphology. In *POMT1* siRNA pre-loaded cells, the morphology recovery is still present with nicely aligned cells that, although increased in cell size, do not display a completely elongated shape. *Scale bars* 20 μM

Discussion

Our results clearly show that, in MSC from different sources, the O-mannosylation-related genes share a common global expression pattern that is conserved through differentiated cell types as fibroblasts and myoblasts, directly deriving from MSC. It has been demonstrated for alpha-dystroglycan that POMGNT2 activity is essential to generate the GalNAc-β3-GlcNAc-β4-Man structure that is further elongated with the repeating disaccharide -α3-GlcA-β3-Xyl-, hereafter referred to as LARGE-glycan due to the enzyme responsible for its synthesis [20]. This structure is a scaffold for alpha-dystroglycan binding to extracellular matrix proteins such as laminin, perlecan, pikachurin, neurexin, and agrin [24, 34, 35]. Interestingly, in both MSC differentiating into muscle progenitors and myoblasts/myotubes *POMGNT2* is clearly upregulated. Increased ER-resident POMGNT2 may then subtract available substrates for the Golgi-resident POMGNT1 and prime the synthesis of the LARGE-glycan branch. This new POMGNT2/POMGNT1 balance may thus explain the high matrix adhesion strength exhibited by myoblasts (detachment pressure: 30 MPa; [36]) where reduction of LARGE-glycan repeats of alpha-dystroglycan during

muscle regeneration was demonstrated to both reduce muscle physiological function and predispose it to dystrophy [22].

A recent publication showed the role of O-mannosylation in conferring functionality not only to alpha-dystroglycan but also to E-cadherin, a member of the Cadherin superfamily [33]. Cadherins are cell adhesion proteins that play a fundamental role in the formation of solid tissues [37–39] and their specific expression often correlates with generation of discrete structures within tissues [40]. In recent years, examples of Cadherins involved in MSC differentiation were presented, with particular attention to N-cadherin whose loss resembles ocular and brain CMD symptoms [41, 42], similar to the neural migration disorder observed in *POMT1* Walker Warburg Syndrome patients [43]. N-cadherin was shown to inhibit MSC osteogenic differentiation through suppressing β-catenin and ERK1/2 signaling pathways [44]. Further, N-cadherin expression and matrix interaction in MSC is strictly required for early chondrogenic differentiation [45, 46]. In addition, in mice, N-cadherin was demonstrated to increase MSC adipocyte differentiation via repression of Wnt5a and Wnt10b adipogenic inhibitors [47]. Most interestingly, O-mannosylation inhibition in MSC resulted in a reduced adipogenic conversion and a complete block of chondrogenic events, whereas the osteogenic potential was increased, suggesting that N-cadherin function might be affected. Furthermore, developing skeletal muscle expresses multiple cadherins, including N-, M-, R-, T-cadherin, and cadherin-11 that altogether cooperates to initiate intracellular signaling events required for the progression of myogenesis [48]. This crucial role is in agreement with the lethal phenotype and detachment observed upon block of O-mannosylation during myogenesis, where cadherin-mediated adhesion and signaling are most likely lost. In this frame, it was recently reported in C2 mouse myogenic cells that recruitment or oligomerization of functional cadherins (N- and E-) in the membrane together with their association with contractile actomyosin fibers in adhesion plaques is crucial to adapt to the rigidity of the intra- and extracellular environments [49]. Moreover, in combination with Cadherins hypoglycosilation-related detrimental effects, the lethal outcome we showed might also be associated with a reduced alpha-dystroglycan activation that was reported to impair the proliferative activity of primary myoblasts [50].

Altogether these results emphasize the crucial role of O-mannosylation for MSC fate, especially in view of tissue formation and homeostasis. Such data are in agreement with the severe phenotypes observed in the individuals affected by O-mannosylation related-CMD. To date, no efficient therapy is available for these diseases. In a recent paper, it was demonstrated that adenovirus-mediated *POMT1* gene transfer can rescue in vitro O-mannosylation defects in *pomt1* mutant fibroblasts [19], although transduction efficiencies of such vectors vary greatly among different cell types and established cell lines. Thus, new approaches are needed and EVs transfer of proteins or mRNA lies in this frame. As a consequence of their origin, EVs are devoid of protein components of intracellular compartments like the ER (where POMT1 and POMT2 reside). Therefore, for these genes only their transcripts can be transferred to recipient cells via EVs. Bruno and coworkers demonstrated that mRNA embedded in EVs can be efficiently translated in recipient cells [51]. Here, we demonstrated for the first time that *POMT1* mRNA-containing BMMSC-EVs can be efficiently incorporated into *pomt1* mutant myoblasts causing a morphology recovery and that a functional O-mannosylation cascade can be, at least partially, restored. siRNA experiments suggested that the phenotype improvement was only in part due to POMT1 activity restoration and that other EVs-associated pathways or molecules may have a crucial role. In this view, microvesicles harbor potential O-mannosylation target as ligand or adhesion molecules that are crucial for the interaction with the environment and contribute to regulate cell shape and morphology. Therefore, a possibility is that some molecules present on MSC-EVs surface may be integrated in the patient myoblast plasma membrane contributing to the phenotype restoration.

In the future, more studies will be needed to confirm EVs transfer not only to myoblasts but also to other affected cell types. In this perspective, recent reports have suggested that EVs administered intravenously [52] or intranasally [53] can cross the blood–brain barrier and deliver the cargo directly into the brain cells. Collectively, these results suggest that MSC-derived EVs offer a new potential therapeutic approach to CMD with an advantage in patient safety because it does not require the use of viral vectors. Also, a crucial point to be stressed is the issue of the content of the vesicles as, in this case, *POMT1* mRNA or other glycosylated proteins or pathways. Even if the active molecules are identified, their potential for clinical use may be greatly affected by their abundance. Moreover, due to the presumable high number of EVs needed to be administrated to patients, different culture conditions able to modify EVs number or content must be explored to define optimal parameters to produce the most effective EVs.

In conclusion, this study emphasizes the crucial role for O-mannosylation in MSC fate and differentiation properties and proposes a proof of concept for a new therapeutic approach to CMD using MSC-derived EVs.

Acknowledgments This project has received funding from European Union's Seventh Programme for research, technological

development and demonstration under grant agreement No. 241879: "Regenerating Bone defects using new biomedical Engineering approaches". The EuroBioBank and Telethon Network of Genetic Biobanks (GTB12001F) are gratefully acknowledged for providing biological samples. The work of M.L. and S.S. was supported by the Deutsche Forschungsgemeinschaft grant SFB1036, project A11 and LO-1807/1-1, respectively.

Compliances with ethical standards

Funding Funding sources had not involvement in study design, data generation or manuscript preparation.

Conflict of interest The authors declare that they have no conflicts of interest.

Ethical standards All procedures performed in studies involving human participants were in accordance with the ethical standards of the institutional and/or national research committee and with the 1964 Helsinki declaration and its later amendments or comparable ethical standards. Informed consent was obtained from all individual participants included in the study.

References

1. Cook D, Genever P (2013) Regulation of mesenchymal stem cell differentiation. Adv Exp Med Biol 786:213–229. doi:10.1007/978-94-007-6621-1_12
2. Bossolasco P, Corti S, Strazzer S, Borsotti C, Del Bo R, Fortunato F, Salani S, Quirici N, Bertolini F, Gobbi A et al (2004) Skeletal muscle differentiation potential of human adult bone marrow cells. Exp Cell Res 295(1):66–78
3. Montelatici E, Baluce B, Ragni E, Lavazza C, Parazzi V, Mazzola R, Cantarella G, Brambilla M, Giordano R, Lazzari L (2014) Defining the identity of human adipose-derived mesenchymal stem cells. Biochem Cell Biol 20:1–9
4. Pittenger MF, Mackay AM, Beck SC, Jaiswal RK, Douglas R, Mosca JD, Moorman MA, Simonetti DW, Craig S, Marshak DR (1999) Multilineage potential of adult human mesenchymal stem cells. Science 284:143–147
5. Uezumi A, Ojima K, Fukada S, Ikemoto M, Masuda S, Miyagoe-Suzuki Y, Takeda S (2006) Functional heterogeneity of side population cells in skeletal muscle. Biochem Biophys Res Commun 341:864–873
6. Laino G, Graziano A, d'Aquino R, Pirozzi G, Lanza V, Valiante S, De Rosa A, Naro F, Vivarelli E, Papaccio G (2006) An approachable human adult stem cell source for hard-tissue engineering. J Cell Physiol 206:693–701
7. De Bari C, Dell'Accio F, Tylzanowski P, Luyten FP (2001) Multipotent mesenchymal stem cells from adult human synovial membrane. Arthritis Rheum 44:1928–1942
8. Wang HS, Hung SC, Peng ST, Huang CC, Wei HM, Guo YJ, Fu YS, Lai MC, Chen CC (2004) Mesenchymal stem cells in the Wharton's jelly of the human umbilical cord. Stem Cells 22:1330–1337
9. Romanov YA, Svintsitskaya VA, Smirnov VN (2003) Searching for alternative sources of postnatal human mesenchymal stem cells: candidate MSC-like cells from umbilical cord. Stem Cells 21:105–110
10. Barilani M, Lavazza C, Viganò M, Montemurro T, Boldrin V, Parazzi V, Montelatici E, Crosti M, Moro M, Giordano R et al (2015) Dissection of the cord blood stromal component reveals predictive parameters for culture outcome. Stem Cells Dev 24(1):104–114. doi:10.1089/scd.2014.0160
11. Bernardo ME, Fibbe WE (2012) Safety and efficacy of mesenchymal stromal cell therapy in autoimmune disorders. Ann N Y Acad Sci 1266:107–117. doi:10.1111/j.1749-6632.2012.06667.x. Review
12. Boregowda SV, Phinney DG (2012) Therapeutic applications of mesenchymal stem cells: current outlook. BioDrugs 26(4):201–208. doi:10.2165/11632790-000000000-00000
13. György B, Hung ME, Breakefield XO, Leonard JN (2015) Therapeutic applications of extracellular vesicles: clinical promise and open questions. Annu Rev Pharmacol Toxicol 55:439–464. doi:10.1146/annurevEVs-pharmtox-010814-124630
14. Roth Z, Yehezkel G, Khalaila I (2012) Identification and quantification of protein glycosylation. Int J Carbohydr Chem 2012. doi:10.1155/2012/640923
15. Varki A, Cummings RD, Esko JD, Freeze HH, Stanley P, Bertozzi CR, Hart GW, Etzler ME (eds) (2009) Essentials of glycobiology, Chapter 6, 2nd edn. Cold Spring Harbor Laboratory Press, Cold Spring Harbor. ISBN-13: 9780879697709
16. Hamouda H, Ullah M, Berger M, Sittinger M, Tauber R, Ringe J, Blanchard V (2013) N-glycosylation profile of undifferentiated and adipogenically differentiated human bone marrow mesenchymal stem cells: towards a next generation of stem cell markers. Stem Cells Dev 22(23):3100–3113. doi:10.1089/scd.2013.0108
17. Wells L (2013) The o-mannosylation pathway: glycosyltransferases and proteins implicated in congenital muscular dystrophy. J Biol Chem 288(10):6930–6935. doi:10.1074/jbc.R112.438978
18. Manya H, Chiba A, Yoshida A, Wang X, Chiba Y, Jigami Y, Margolis RU, Endo T (2004) Demonstration of mammalian protein O-mannosyltransferase activity: coexpression of POMT1 and POMT2 required for enzymatic activity. Proc Natl Acad Sci USA 101(2):500–505
19. Willer T, Lee H, Lommel M, Yoshida-Moriguchi T, de Bernabe DB, Venzke D, Cirak S, Schachter H, Vajsar J, Voit T (2012) ISPD loss-of-function mutations disrupt dystroglycan O-mannosylation and cause Walker-Warburg syndrome. Nat Genet 44:575–580
20. Endo T (2015) Glycobiology of α-dystroglycan and muscular dystrophy. J Biochem 157(1):1–12. doi:10.1093/jb/mvu066
21. Winder SJ (2001) The complexities of dystroglycan. Trends Biochem Sci 26:118–124
22. Goddeeris MM, Wu B, Venzke D, Yoshida-Moriguchi T, Saito F, Matsumura K, Moore SA, Campbell KP (2013) LARGE glycans on dystroglycan function as a tunable matrix scaffold to prevent dystrophy. Nature 503(7474):136–140. doi:10.1038/nature12605
23. Yoshida-Moriguchi T, Willer T, Anderson ME, Venzke D, Whyte T, Muntoni F, Lee H, Nelson SF, Yu L, Campbell KP (2013) SGK196 is a glycosylation-specific O-mannose kinase required for dystroglycan function. Science 341(6148):896–899. doi:10.1126/science.1239951
24. Inamori K, Yoshida-Moriguchi T, Hara Y, Anderson ME, Yu L, Campbell KP (2012) Dystroglycan function requires xylosyl- and glucuronyltransferase activities of LARGE. Science 335:93–96
25. Willer T, Inamori K, Venzke D, Harvey C, Morgensen G, Hara Y, Valero Beltrán, de Bernabé D, Yu L, Wright KM, Campbell KP (2014) The glucuronyltransferase B4GAT1 is required for initiation of LARGE-mediated α-dystroglycan functional glycosylation. Elife 3. doi:10.7554/eLife.03941
26. Yoshida-Moriguchi T, Willer T, Anderson ME, Venzke D, Whyte T, Muntoni F, Lee H, Nelson SF, Yu L, Campbell KP (2013) SGK196 is a glycosylation-specific O-mannose kinase required for dystroglycan function. Science 341(6148):896–899. doi:10.1126/science.1239951
27. Inamori K, Endo T, Gu J, Matsuo I, Ito Y, Fujii S, Iwasaki H, Narimatsu H, Miyoshi E, Honke K, Taniguchi N (2004) N-Acetylglucosaminyltransferase IX acts on the GlcNAc beta

1,2-Man alpha 1-Ser/Thr moiety, forming a 2,6-branched structure in brain O-mannosyl glycan. J Biol Chem 279(4):2337–2340
28. Ragni E, Montemurro T, Montelatici E, Lavazza C, Viganò M, Rebulla P, Giordano R, Lazzari L (2013) Differential microRNA signature of human mesenchymal stem cells from different sources reveals an "environmental-niche memory" for bone marrow stem cells. Exp Cell Res 319(10):1562–1574. doi:10.1016/j.yexcr.2013.04.002
29. Ragni E, Viganò M, Rebulla P, Giordano R, Lazzari L (2013) What is beyond a qRT-PCR study on mesenchymal stem cell differentiation properties: how to choose the most reliable housekeeping genes. J Cell Mol Med 17(1):168–180. doi:10.1111/j.1582-4934.2012.01660.x
30. Rojek JM, Campbell KP, Oldstone MB, Kunz S (2007) Old World arenavirus infection interferes with the expression of functional alpha-dystroglycan in the host cell. Mol Biol Cell 18(11):4493–4507
31. Orchard MG, Neuss JC, Galley CM, Carr A, Porter DW, Smith P, Scopes DI, Haydon D, Vousden K, Stubberfield CR et al (2004) Rhodanine-3-acetic acid derivatives as inhibitors of fungal protein mannosyl transferase 1 (PMT1). Bioorg Med Chem Lett 14(15):3975–3978
32. Arroyo J, Hutzler J, Bermejo C, Ragni E, García-Cantalejo J, Botías P, Piberger H, Schott A, Sanz AB, Strahl S (2011) Functional and genomic analyses of blocked protein O-mannosylation in baker's yeast. Mol Microbiol 79(6):1529–1546. doi:10.1111/j.1365-2958.2011.07537.x
33. Lommel M, Winterhalter PR, Willer T, Dahlhoff M, Schneider MR, Bartels MF, Renner-Müller I, Ruppert T, Wolf E, Strahl S (2013) Protein O-mannosylation is crucial for E-cadherin-mediated cell adhesion. Proc Natl Acad Sci USA 110(52):21024–21029. doi:10.1073/pnas.1316753110
34. Yoshida-Moriguchi T, Yu L, Stalnaker SH, Davis S, Kunz S, Madson M, Oldstone MB, Schachter H, Wells L, Campbell KP (2010) O-mannosyl phosphorylation of alpha-dystroglycan is required for laminin binding. Science 327:88–92
35. Dobson CM, Hempel SJ, Stalnaker SH, Stuart R, Wells L (2013) OMannosylation and human disease. Cell Mol Life Sci 70(16):2849–2857. doi:10.1007/s00018-012-1193-0
36. Yoshikawa HY, Kawano T, Matsuda T, Kidoaki S, Tanaka MJ (2013) Morphology and adhesion strength of myoblast cells on photocurable gelatin under native and non-native micromechanical environments. Phys Chem B 117(15):4081–4088. doi:10.1021/jp4008224
37. Takeichi M (1995) Morphogenetic roles of classic cadherins. Curr Opin Cell Biol 7:619–627
38. Tepass U (1999) Genetic analysis of cadherin function in animal morphogenesis. Curr Opin Cell Biol 11:540–548
39. Gumbiner BM (2005) Regulation of cadherin-mediated adhesion in morphogenesis. Nat Rev Mol Cell Biol 6:622–634
40. Gumbiner BM (1996) Cell adhesion: the molecular basis of tissue architecture and morphogenesis. Cell 84:345–357
41. Erdmann B, Kirsch FP, Rathjen FG, Moré MI (2003) N-cadherin is essential for retinal lamination in the zebrafish. Dev Dyn 226(3):570–577
42. Kadowaki M, Nakamura S, Machon O, Krauss S, Radice GL, Takeichi M (2007) N-cadherin mediates cortical organization in the mouse brain. Dev Biol 304(1):22–33
43. Beltrán-Valero de Bernabé D, Currier S, Steinbrecher A, Celli J, van Beusekom E, van der Zwaag B, Kayserili H et al (2002) Mutations in the O-mannosyltransferase gene POMT1 give rise to the severe neuronal migration disorder Walker-Warburg syndrome. Am J Hum Genet 71(5):1033–1043
44. Xu L, Meng F, Ni M, Lee Y, Li G (2013) N-cadherin regulates osteogenesis and migration of bone marrow-derived mesenchymal stem cells. Mol Biol Rep 40(3):2533–2539. doi:10.1007/s11033-012-2334-0
45. Oberlender SA, Tuan RS (1994) Expression and functional involvement of N-cadherin in embryonic limb chondrogenesis. Development 120(1):177–187
46. Bian L, Guvendiren M, Mauck RL, Burdick JA (2013) Hydrogels that mimic developmentally relevant matrix and N-cadherin interactions enhance MSC chondrogenesis. Proc Natl Acad Sci USA 110(25):10117–10122. doi:10.1073/pnas.1214100110
47. Haÿ E, Dieudonné FX, Saidak Z, Marty C, Brun J, Da Nascimento S, Sonnet P, Marie PJ (2014) N-cadherin/wnt interaction controls bone marrow mesenchymal cell fate and bone mass during aging. J Cell Physiol 229(11):1765–1775. doi:10.1002/jcp.24629
48. Redfield A, Nieman MT, Knudsen KA (1997) Cadherins promote skeletal muscle differentiation in threedimensional cultures. J Cell Biol 138:1323–1331
49. Ladoux B, Anon E, Lambert M, Rabodzey A, Hersen P, Buguin A, Silberzan P, Mège RM (2010) Strength dependence of cadherin-mediated adhesions. Biophys J 98(4):534–542. doi:10.1016/j.bpj.2009.10.044
50. Miyagoe-Suzuki Y, Masubuchi N, Miyamoto K, Wada MR, Yuasa S, Saito F, Matsumura K, Kanesaki H, Kudo A, Manya H, Endo T, Takeda S (2009) Reduced proliferative activity of primary POMGnT1-null myoblasts in vitro. Mech Dev 126(3–4):107–116. doi:10.1016/j.mod.2008.12.001
51. Bruno S, Grange C, Deregibus MC, Calogero RA, Saviozzi S, Collino F, Morando L, Busca A, Falda M, Bussolati B, Tetta C, Camussi G (2009) Mesenchymal stem cell-derived microvesicles protect against acute tubular injury. J Am Soc Nephrol 20(5):1053–1067. doi:10.1681/ASN.2008070798
52. Alvarez-Erviti L, Seow Y, Yin H, Betts C, Lakhal S, Wood MJ (2011) Delivery of siRNA to the mouse brain by systemic injection of targeted exosomes. Nat Biotechnol 29(4):341–345. doi:10.1038/nbt.1807
53. Zhuang X, Xiang X, Grizzle W, Sun D, Zhang S, Axtell RC, Ju S, Mu J, Zhang L, Steinman L et al (2011) Treatment of brain inflammatory diseases by delivering exosome encapsulated anti-inflammatory drugs from the nasal region to the brain. Mol Ther 19(10):1769–1779. doi:10.1038/mt.2011.164